Astron. Astrophys. 88, 175–183 (1980)

ASTRONOMY
AND
ASTROPHYSICS

21 cm Maps of Jupiter's Radiation Belts from all Rotational Aspects

Imke de Pater

Sterrewacht Leiden, Postbus 9513, NL-2300 RA Leiden, The Netherlands

Received August 8, 1979

Summary. Two-dimensional maps of the radio emission from Jupiter were made in December 1977 at a frequency of 1,412 MHz using the Westerbork telescope in the Netherlands. Pictures in all four Stokes parameters have been obtained every 15° in longitude, each smeared over 15° of the planet's rotation. The maps have an E–W resolution of ~1/3 of the diameter of the disk and a N–S resolution 3 times less. The total intensity and linear polarization maps are accurate to 0.5% and the circularly polarized maps to 0.1% of the maximum intensities in *I*. The whole set of maps clearly show the existence of higher order terms in the magnetic field of Jupiter.

Key words: Jupiter – circular polarization – (multipole) magnetic field

1. Introduction

Previous observations of Jupiter using the Westerbork Synthesis Radio Telescope at the frequencies 610, 1,415, and 4,995 MHz (de Pater and Dames, 1979; henceforth referred to as Paper I) gave a good picture of the general distribution of the emission from the radiation belts and disk of the planet. However as we pointed out, they were not as accurate as we desired and knew to be possible with the instrument, due to the low declination of Jupiter at that time. In particular, we were not able to measure the circular polarization, a vital parameter for evaluating models of the magnetic field of Jupiter, nor could we obtain much north-south resolution. Finally there was a need to ascertain possible longitudinal motions of a "hot" region in Jupiter's magnetosphere first found by Branson (1968) and confirmed in Paper I. We therefore observed this planet again in December 1977 when it was at its most northerly opposition to the earth. Pictures were obtained at a frequency of 1,412 MHz in all four Stokes parameters at 24 different rotational aspects of the planet, each integrated over 15° of Jovian rotation. The maps clearly show the complex structure of the radiation belt close to the planet which may be interpreted in terms of a multipole magnetic field structure.

2. Observing and Reduction Technique

The properties of the Westerbork telescope and its operation have been described extensively elsewhere (Högbom and Brouw, 1974; Baars and Hooghoudt, 1974; Casse and Muller, 1974; Brouw, 1975). Since we observed Jupiter when it was at its most northerly opposition to the earth we could really make two-dimensional pictures of the planet at all rotational aspects, smeared over 15° of Jovian rotation with a resolution of $0.7\,R_j$ in RA (R_j=Jovian radius). In order to get resolution in both RA and Dec directions one needs a good coverage of the Fourier transform (UV) plane.

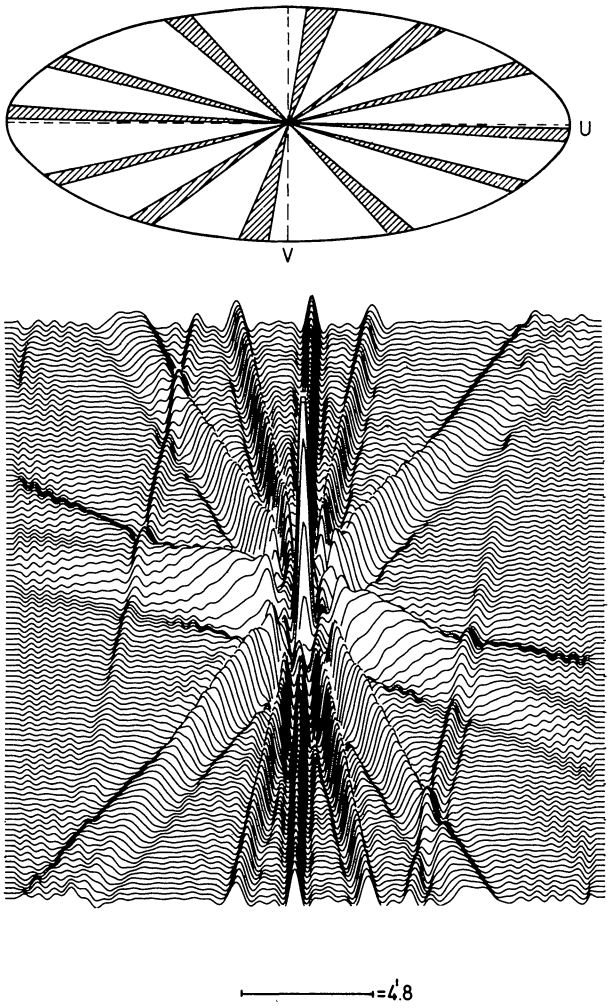

Fig. 1a and b. Part **a** shows schematically the filling of the Fourier transform plane used to map Jupiter according to the method described in the text. The coordinates *U* (east-west) and *V* (north-south) refer to the length of a baseline projected onto the sky. Part **b** shows a typical beam pattern for our observations

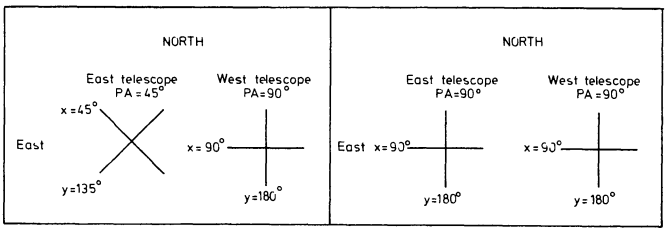

Fig. 2a and b. Dipoles for the **a** "crossed" and **b** "parallel" configuration (after Weiler, 1973; Weiler and Raimond, 1976). Each telescope has the two dipoles x and y

We therefore made 12 h observations on 5 consecutive days (Dec. 16–21 1977; in fact one extra observation of 7 h was made on the day before) which, when cut into pieces of 25 min, gave 6 short observations at each rotational aspect equally spread in hour angle. Figure 1 shows very schematically the filling of the UV plane used to map Jupiter at each longitude.

Since the circularly polarized flux contains much information concerning the magnetic field of the planet we decided to use a dipole configuration such that all dipoles per interferometer were parallel at position angle $PA=90°$. It appears that using this configuration the complex visibility function of the Stokes parameters V and U will be measured with a much better accuracy than normally achieved with a "crossed" dipole configuration (dipoles of the western telescopes of each interferometer pair at $PA=90°$, those of the eastern telescopes at $PA=45°$, see Fig. 2) (Weiler and Raimond, 1976). The complex outputs R of the four channels of an interferometer with the "crossed" configuration can be written as (Weiler, 1973):

$$R_{xx}=\frac{1}{2\sqrt{2}}G_{xx}(I\{1-\Delta_{xx}^{-}+i\theta_{xx}^{+}\}-Q\{1+\Delta_{xx}^{+}-i\theta_{xx}^{-}\}$$
$$+U\{1-\Delta_{xx}^{+}+i\theta_{xx}^{-}\}-iV\{1+\Delta_{xx}^{-}-i\theta_{xx}^{+}\}),$$
$$R_{xy}=\frac{1}{2\sqrt{2}}G_{xy}(I\{1+\Delta_{xy}^{-}-i\theta_{xy}^{+}\}-Q\{1-\Delta_{xy}^{+}+i\theta_{xy}^{-}\}$$
$$-U\{1+\Delta_{xy}^{+}-i\theta_{xy}^{-}\}+iV\{1-\Delta_{xy}^{-}+i\theta_{xy}^{+}\}),$$
$$R_{yx}=\frac{-1}{2\sqrt{2}}G_{yx}(I\{1+\Delta_{yx}^{-}-i\theta_{yx}^{+}\}+Q\{1-\Delta_{yx}^{+}+i\theta_{yx}^{-}\}$$
$$+U\{1+\Delta_{yx}^{+}-i\theta_{yx}^{-}\}+iV\{1-\Delta_{yx}^{-}+i\theta_{yx}^{+}\}),$$
$$R_{yy}=\frac{1}{2\sqrt{2}}G_{yy}(I\{1-\Delta_{yy}^{-}+i\theta_{yy}^{+}\}+Q\{1+\Delta_{yy}^{+}-i\theta_{yy}^{-}\}$$
$$-U\{1-\Delta_{yy}^{+}+i\theta_{yy}^{-}\}-iV\{1+\Delta_{yy}^{-}-i\theta_{yy}^{+}\}),$$

where the G's are the complex instrumental gain factors, $\Delta^{-}=\Delta_W-\Delta_E$ are errors in the dipole setting of the Western and Eastern telescopes, i.e. an instrumental linear polarization, and $\theta^{+}=\theta_W+\theta_E$ represents an instrumental circular polarization. Both terms Δ and θ can be adjusted to a level of $\lesssim 1\%$ of I (Weiler, 1973). Neglecting these small terms in the solution for the four Stokes parameters cause errors of the order of 0.4% of I in the individual maps. Fluctuations in the system gains are of the order of $\lesssim 1\%$ of the receiver output, giving a total error of $\sim 0.5\%$ of I in all maps.

With the dipoles of all telescopes set parallel to each other at position angles 90° one can write the complex outputs R' of the four channels of an interferometer as (Weiler and Raimond, 1976):

$$R'_{xx}=\tfrac{1}{2}G_{xx}\{I-Q-U(\Delta_{xx}^{+}-i\theta_{xx}^{-})-iV(\Delta_{xx}^{-}-i\theta_{xx}^{+})\},$$
$$R'_{xy}=\tfrac{1}{2}G_{xy}\{I(\Delta_{xy}^{-}-i\theta_{xy}^{+})+Q(\Delta_{xy}^{+}-i\theta_{xy}^{-})-U+iV\},$$
$$R'_{yx}=-\tfrac{1}{2}G_{yx}\{I(\Delta_{yx}^{-}-i\theta_{yx}^{+})-Q(\Delta_{yx}^{+}-i\theta_{yx}^{-})+U+iV\},$$
$$R'_{yy}=\tfrac{1}{2}G_{yy}\{I+Q+U(\Delta_{yy}^{+}-i\theta_{yy}^{-})-iV(\Delta_{yy}^{-}-i\theta_{yy}^{+})\}.$$

Neglecting the terms (U, Q, V). (Δ, θ) in this configuration causes errors of 0.1% of I in the various maps and according to Weiler and Raimond (1976) we can write the receiver output as:

$$R'_{xx}=\tfrac{1}{2}G_{xx}(I-Q),$$
$$R'_{xy}=\tfrac{1}{2}G_{xy}(I\varepsilon_{xy}-U+iV),$$
$$R'_{yx}=-\tfrac{1}{2}G_{xy}(I\varepsilon_{yx}+U+iV),$$
$$R'_{yy}=\tfrac{1}{2}G_{yy}(I+Q),$$

where $\varepsilon=(\Delta^{-}-i\theta^{+})$, a complex instrumental error which can be determined from calibration measurements as shown below. Together with the fact that possible gain fluctuations in the system are $\lesssim 1\%$ of the received signals it will be clear that the uncertainties in U and V generated by system errors causing "leakage" of I will be $\sim 0.1\%$ of I or less.

To calibrate the Jovian data we chose the observing sequence shown in Table 1. The parameters of the calibration sources are in Table 2. After correction for known instrumental and sky effects (van Someren Greve, 1974), we have used the adopted flux of 3C147 to define the gain of the system assuming zero polarization for this source (Wilson and Weiler, 1976). The other three sources listed were used for geometry and phase calibrations. The complex correction factors G_{xx} and G_{yy} could be determined directly from the calibrations taken in the "parallel" configuration. Using also the calibration observations taken with the "crossed" configuration the G_{yx} and G_{xy} for each observation could be determined due to the fact that the mutual channels of one baseline are very stable (relative drifts of the 4 channels of a given baseline over 24 h are less than 1% in amplitude and 0°.5 in phase). The observations

Table 1. Jovian observing sequence in December 1977

Sidereal day	Source	Observation time in min.	dipole configuration
350	3C48	40	x+
	3C286	15	x+
351	3C147	20	++
	Jupiter I	7hr 1 min	
	3C286	30	
	3C48	40	
	3C147	22	
352	Jupiter 2	12hr 4 min	
	3C286	60	
	3C309.1	60	
	3C48	220	
	3C147	22	
353	Jupiter 3	12hr 4 min	
	3C286	7hr 12 min	
	3C309.1	83	
	3C48	139	
	3C147	20	
354	Jupiter 4	12hr 4 min	
	3C286	60	
	3C48	45	
	3C147	20	
355	Jupiter 5	12hr 4 min	
	3C286	60	
	3C48	25	
	3C147	20	
356	Jupiter 6	12hr 4 min	
	3C286	60	++
	3C286	60	x+
	3C48	40	
357	3C147	120	
	3C48	120	
	3C147	90	
	3C48	135	
	3C286	83	x+

Table 2. Calibration sources. The flux densities of 3C48, 3C286, and 3C309.1 are "mean" flux densities, derived from ratio's to the flux density of 3C147 (typical errors $\sim 10^{-3}$). Column 5 shows measured values for the degree of linear polarization P_L and the position angle of the electric vector PA (corrected for Faraday rotation in the earth's ionosphere). Column 6 shows values for the polarization of these sources published by Berge and Seielstad (1972) and Morris and Berge (1964) respectively

Source	RA	Dec	flux (21cm) (Jy)	P_L, PA	P_L, PA (published values at 21 cm)	
3C147	$5^h38^m43^s.5$	49°49'42".9	21.57			0.6±0.3% ; 0.2±0.5% 173°±10° ; 138±57°
3C48	1 34 49.8	32 54 20.6	15.67	0.52±0.08% 115°±5°	0.43±0.07% 139°7±4°8	0.6±0.6% ; 0.7±0.6% 154°±28° ; 162°±25°
3C286	13 28 49.7	39 45 58.8	14.30	9.28±0.04% 29°.1±1°.0	9.36±0.07% 32°.0±1°.1	9.3±0.5% 32°±2°
3C309.1	14 58 56.6	71 52 11.2	7.88			

of the unpolarized source 3C147 provided the complex instrumental error terms ε_{xy} and ε_{yx}. The Fourier components of the four Stokes parameters for each inferometer can then be represented by:

$$I=\tfrac{1}{2}(xx+yy) \qquad Q=\tfrac{1}{2}(yy-xx),$$

$$U=\tfrac{1}{4}\{-2xy+2yx+(\varepsilon_{xy}-\varepsilon_{yx})xx+(\varepsilon_{xy}-\varepsilon_{yx})yy\},$$

$$V=-\frac{i}{4}\{2xy+2yx-(\varepsilon_{xy}+\varepsilon_{yx})xx-(\varepsilon_{xy}+\varepsilon_{yx})yy\},$$

where xx, xy, yx, and yy are the fully corrected complex receiver outputs. It appeared that the maximum circularly polarized intensities remaining in the measurements of 3C286 and 3C48 were less than 0.1% of the maximum intensities of I; thus the instrumental error in the V maps is indeed less than 0.1% of I. The degree of linear polarization P_L and the position angles of the electric vector P_A for 3C286 and 3C48 are shown in Table 2, Column 5. The position angles are corrected for Faraday rotation in the earth's ionosphere (3° and 2° respectively) using electron density data obtained from the Royal Dutch Meteorological Institute in De Bilt. Column 6 shows values for P_L and P_A at 21 cm published by Berge and Seielstad (1972) and Morris and Berge (1964); these position angles are not corrected for Faraday rotation which will cause an additional error of $\lesssim 5°$ (Weiler and Raimond, 1976). The polarization of 3C286 is in excellent agreement with these published values. Observations of 3C147 and 3C48 show very small values for the degree of linear polarization so it will be clear that these numbers and in particular the position angles largely depend on the chosen polarization of the calibration source.

After all data were properly corrected, background sources were subtracted using the standard reduction programs. Then the motion of Jupiter along the sky was removed by moving the phase reference point in the same way the planet moved along the sky. Since the planet only moved 4′ during 12 h there is hardly any primary beam attenuation in the data.

At the time of observation, Jupiter was at a distance of 4.1525 AU from the earth, so that the measured flux densities were multiplied by a factor of $(4.1525/4.04)^2$ to correct them to those at the standard distance of 4.04 AU. Before Fourier transforming the combined UV points, we chose a grid size such that there were 4–5 grid points per half power beam width and no (aliased) grating ring of the synthesized beam pattern could distort our source. This size came out to be 4".186 in RA and larger by a factor of cosec δ in Dec. To remove the effects of the antenna pattern from the maps we used the procedure CLEAN, a deconvolution technique developed by Högbom (1974). The components were restored afterwards to the maps using a Gaussian shaped beam with a half power beam width of 16".6 in RA, which is 15% less than the synthesized half power beam width. By choosing this smaller value one can try to regain some of the resolution suppressed in the map making process due to the rather strong taper of the intensities contributed for the longest baselines (Gaussian with a value of 0.25 at the longest baseline). How small a beam size may be chosen depends upon the quality of the maps, as long as it is larger than $\sim 0.5\,\lambda/L_{max}$, where L_{max} is the maximum baseline in wavelengths, λ. In our observing period, $0.5\,\lambda/L_{max}$ was about 13".7. A width of 16".6 (which is $0.7\,R_j$ at the time of observation) appeared to be an optimal choice for our maps. The larger beam in Dec. is just slightly less than the N–S extent of the disk. The smearing effect on the data due to the integration over 15° of Jovian rotation amounts to $\sim 12".5$ at $2\,R_j$.

It appeared that we had to be very careful using CLEAN for those maps which contain both positive and negative components, due to the rather "dirty" beam pattern with large negative side lobes caused by the large unsampled parts of the UV plane (an example of a beam at one Jovian longitude is shown in Fig. 1b). We could obtain satisfactory results for the Q maps only by handling maps of the xx and yy channels separately, both of which are positive definite. For the U maps we could not use the "trick" of cleaning only positive definite maps but even without this, the errors in these low intensity maps appeared to be of the same order as in the Q maps. The noise in the I maps is about 3–5 mJy/beam which is about 0.5% of the maximum intensities; the theoretical noise at the time of observation would be 1.5 mJy/beam for a 3 h observation. The "noise" in the Q maps is about 2 mJy/beam and in the U maps 3 mJy/beam. The resulting noise in the map of the polarized intensity $(Q^2+U^2)^{1/2}$ is ~ 4 mJy/beam which is $\sim 1\%$ of the maximum intensities in these maps. As predicted by the theory referred to above, the V maps indeed appeared to be accurate to 0.1% of the maximum intensities in the I maps; the noise here is about 1 mJy/beam.

The position angles of the electric vectors determined were corrected for Faraday rotation in the earth's ionosphere using electron density data obtained from the Dutch meteorological institute in De Bilt. This correction was 1°.43 with variations up to 20–30%. The error possibly remaining in the position angles is $\sim 0°.5$.

3. Results

3.1. Integrated Jovian Parameters

Figures 3 and 4 show various parameters of the integrated Jovian radiation as functions of, respectively, Jovian magnetic longitude

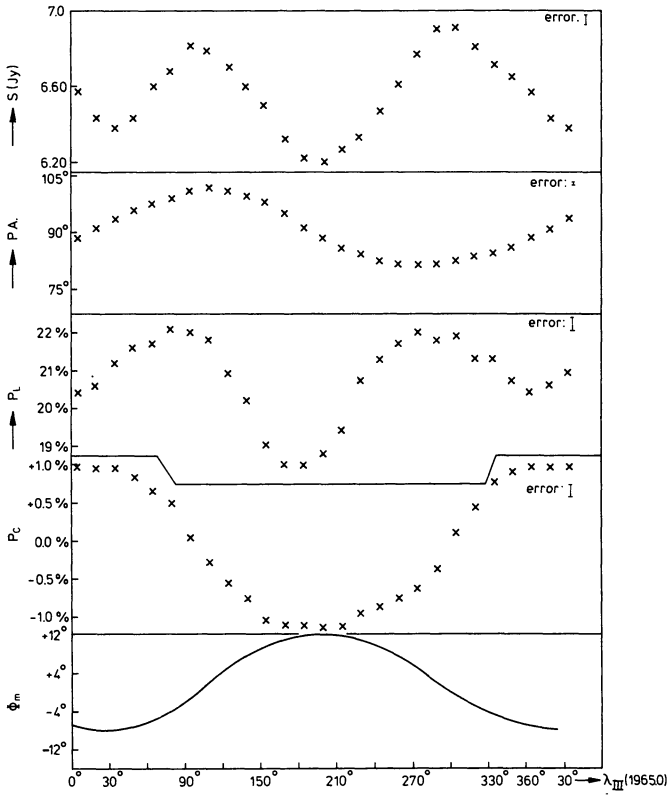

Fig. 3a–e. Various parameters of the integrated radiation of Jupiter at 21 cm as functions of the magnetic longitude of Jupiter (in Syst. III 1965.0). The north magnetic pole is at 201°. **a** Total integrated flux. **b** Position angle of the electric vector measured eastward from north in the sky. **c** Degree of linear polarization. **d** Degree of circular polarization. **e** Magnetic latitude of the earth with respect to Jupiter

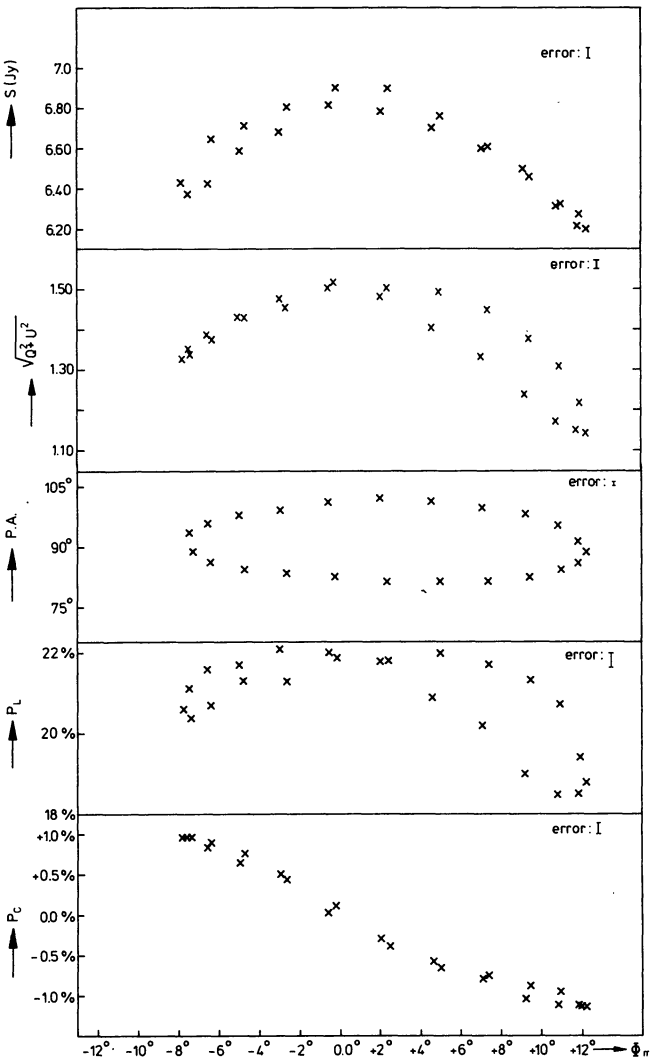

Fig. 4a–e. The parameters of the integrated radiation of Jupiter (see Fig. 3) as functions of the magnetic latitude of the earth with respect to Jupiter. **a** Total integrated flux. **b** Polarized flux density. **c** Position angle of the electric vector. **d** Degree of linear polarization. **e** Degree of circular polarization

λ_{III}(1965.0) and magnetic latitude Φ_m of the earth with respect to Jupiter. The parameters are calculated by integrating the two-dimensional Jovian maps in I, Q, U, and V, which are all averaged over 15° intervals in longitude.

Indicated are:

a) the total integrated flux density, S, in Jy,

b) the polarized flux density, $(Q^2+U^2)^{1/2}$, in Jy (in Fig. 4 only),

c) polarization direction: the position angle of the electric vector, PA, measured eastward from north in the sky (corrected for Faraday rotation in the earth's ionosphere),

d) degree of linear polarization, P_L,

e) degree of circular polarization, P_c,

f) the magnetic latitude of the earth with respect to Jupiter (in Fig. 3 only). This latitude was calculated according to the formula $\Phi_m = D_E + \beta \cos(\lambda_{III} - \lambda_0)$ (Berge and Gulkis, 1976). D_E is the declination of the earth relative to Jupiter's rotational equator (+2°.24 at this epoch), β is the angle between Jupiter's magnetic and rotational axes taken as 10°, and λ_0 is the central meridian longitude of the magnetic north pole taken as 201° (Syst. III 1965.0).

Thinking of a dipole field in which the electron pitch angle distribution is concentrated towards 90° one expects to find a beaming pattern in the various parameters dependent upon the magnetic latitude of the earth, ϕ_m (Morris and Berge, 1962; Roberts and Komesaroff, 1965; Thorne, 1963, 1965; Clarke, 1970). The variation with longitude shown in Fig. 3 is indeed consistent with such a pattern; it shows maxima in S and P_L and zero values in P_c at $\lambda_{III} \sim 100°$ and 300° where $\phi_m \sim 0°$. A real minimum is seen in the first 2 parameters at $\lambda_{III} \sim 200°$ where ϕ_m has its maximum, due to D_E being positive at the time our observations were made. The difference in height between the two maxima in S has been detected before (see Berge and Gulkis, 1976); in 1973, however, it was much more pronounced, as shown in Paper I. If this difference is caused by the existence of a kind of "hot" region near longitude 250°–260° as was suggested in that paper the variations in the ratio between the two maxima with time may be due to geometrical effects; i.e. distortions of the magnetic equatorial plane (Conway and Stannard, 1972; Gerard, 1976) will cause additional beaming effects depending upon the angle of the line of sight with the local (distorted) magnetic equatorial plane.

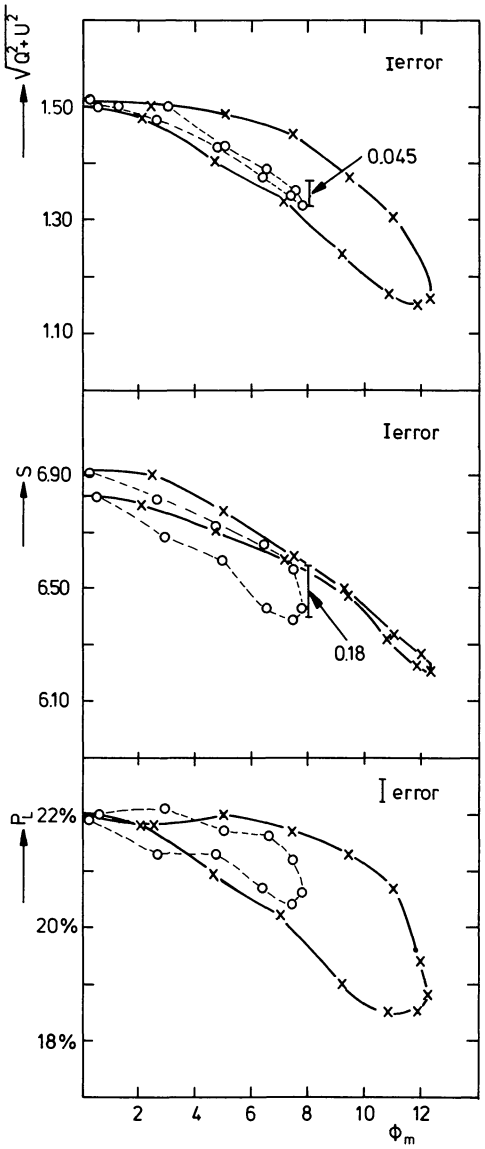

Fig. 5a–c. The parameters **a** S, **b** $(Q^2+U^2)^{1/2}$ and **c** P_L of the integrated radiation from Jupiter as functions of the magnetic latitude Φ_m of the earth. Points measured at southern latitudes are indicated by circles and connected by a dotted line; the curves with crosses represent measurements at northern latitudes. The number indicated in **a** and **b** shows the difference in flux density between averages of the two curves at $\phi_m = 7°.8$

The value of P_c at $\lambda_{III} \sim 200°$ is only slightly higher than at $\lambda_{III} \sim 20°$ which is clarified in Fig. 4 by the flattening of the curve at both ends of ϕ_m as found by many other people (e.g. Neidhöfer et al., 1977). The shape of this curve is determined by the pitch angle distribution of the electrons (Roberts and Komesaroff, 1976) which in general can be written by a sum of terms $\sum_q A_q k_q \sin^q \alpha_e$, where α_e is the equatorial pitch angle, k_q is defined such that $\int_0^\pi k_q \sin^q(\alpha_e) 2\pi \sin(\alpha_e) d\alpha_e = 1$ and $\sum_q A_q = 1$ (Clarke, 1970). When $q=0$, the distribution is isotropic; larger values of q specify more equatorially confined distributions. Roberts and Komesaroff point out that to fit the beaming of the radiation and the curves for linear and circular polarization they need two terms: $q_1 = 1$ and $q_2 \gtrsim 30$ with 29% of the electrons confined to the equator. A fit to our data will be presented in Paper III (see Sect. 3.2).

Figure 4 shows a clear difference in the shape of the curves of S and $(Q^2+U^2)^{1/2}$; values for S at the same ϕ_m at the left side of the curve apparently depend also on the rotational aspects of the planet while for $(Q^2+U^2)^{1/2}$ this same fact is found at the right side. This may be caused by multipole terms in Jupiter's field; the existence of these higher order terms clearly shows up in the two-dimensional maps shown in Sect. 3 and from the Pioneer 11 measurements (Acuna and Ness, 1976; Smith et al., 1976).

It has been known for a long time that there is a variation in the slope of S as a function of ϕ_m between the northern and southern latitudes which depends on D_E. For positive D_E, S falls off more slowly at northern than at southern latitudes; for negative D_E the reverse is true (Roberts and Komesaroff, 1965; Gulkis et al., 1973). This has been interpreted by Degioanni (1974) as being caused by the varying amount of radiation blocked off by the planet at different configurations in space. One would also expect a similar kind of effect in the polarized flux $(Q^2+U^2)^{1/2}$. Figure 5 shows this flux together with S as a function of ϕ_m. Points measured with the earth at southern latitudes are indicated by circles and connected by a dotted line; the curves with crosses represent measurements at northern latitudes. Introducing a quantity Δ according to Degioanni (1974) such that

$$\Delta = (F(\Phi_m = 7°.8) - F(\Phi_m = -7°.8)]/F(\Phi_m = 0°)$$

where F represents the mean flux density at Φ_m we find $\Delta = 0.030 \pm 0.003$ for both S and $(Q^2+U^2)^{1/2}$, which results in $\Delta = 0.0$ for P_L as also shown by the data in Fig. 5. Although the multipole terms in Jupiter's field probably play a major role in defining the shape of the curves in Figs. 4 and 5, this result implies that the slope of the curves indeed will be defined primarily by the blocking effect of the planet.

3.2. *Two-dimensional Jovian Maps*

Figure 6 shows two-dimensional maps of Jupiter at a wavelength of 21 cm. There are 24 different sets of maps of the total intensity, circular and linear polarized flux and a vector diagram of the magnetic field orientation. All maps are averaged over 15° of Jovian rotation. The longitude of the central meridian (Syst. III 1965.0) is indicated in the upper left corner of each set. The vector diagram is obtained by rotating the values of the position angles of the electric vectors by 90°. This represents the direction of the average magnetic field along the line of sight if there is no Faraday rotation within Jupiter's magnetic field, a generally accepted idea which was confirmed in Paper I by comparison of the integrated parameters of the source at $\lambda = 21$ cm and $\lambda = 50$ cm. However for individual parts of the source we have to be more careful. One can write the rotation measure R_m as: $R_m = 2.62\ 10^{-17} \int n_e H\, dl$ where R_m is in radians/cm^2, n_e is the number of non-relativistic electrons/cm^3, H the magnetic field strength along the line of sight in Gauss, and l the position along the line of sight in cm. Using a number density $n_e \sim 50$–100/cm^3 as found for the proton density in the plasmasphere (Frank et al., 1976) and $H \sim 1$ Gauss, we find a Faraday rotation at $\lambda = 21$ cm of about a degree. Thus we can safely neglect this rotation in Jupiter's field, even close to the planet.

The "hot" region found at a longitude of $255° \pm 10°$ in Paper I is clearly visible in the total intensity maps: to facilitate intercomparison between the maps the contours belonging to the

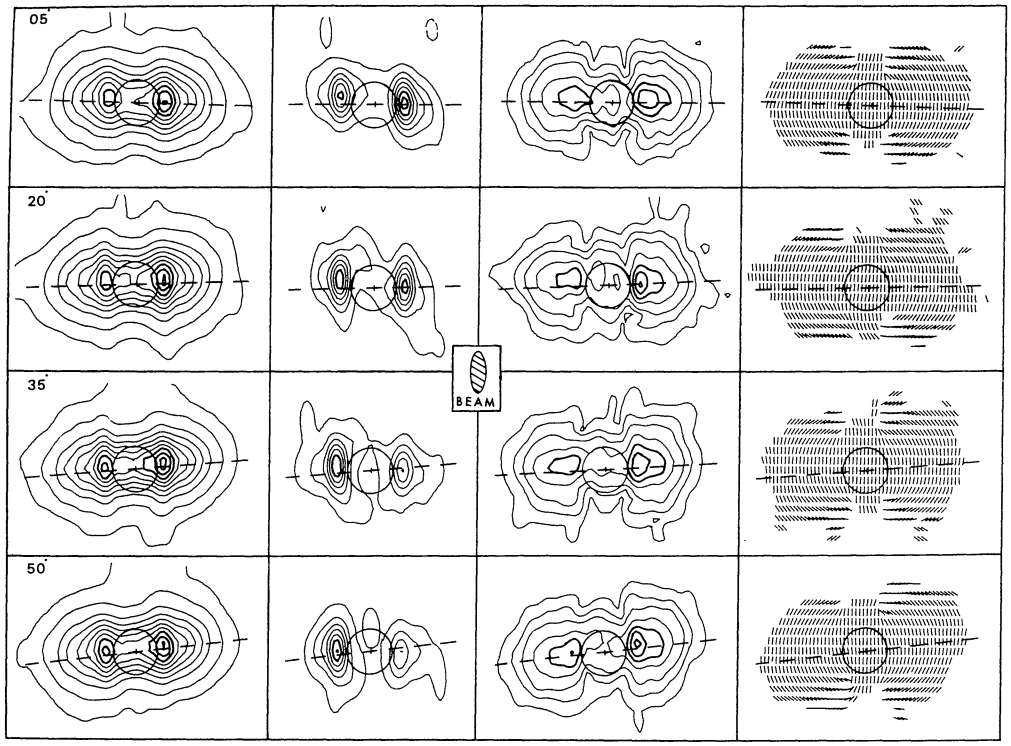

Fig. 6a

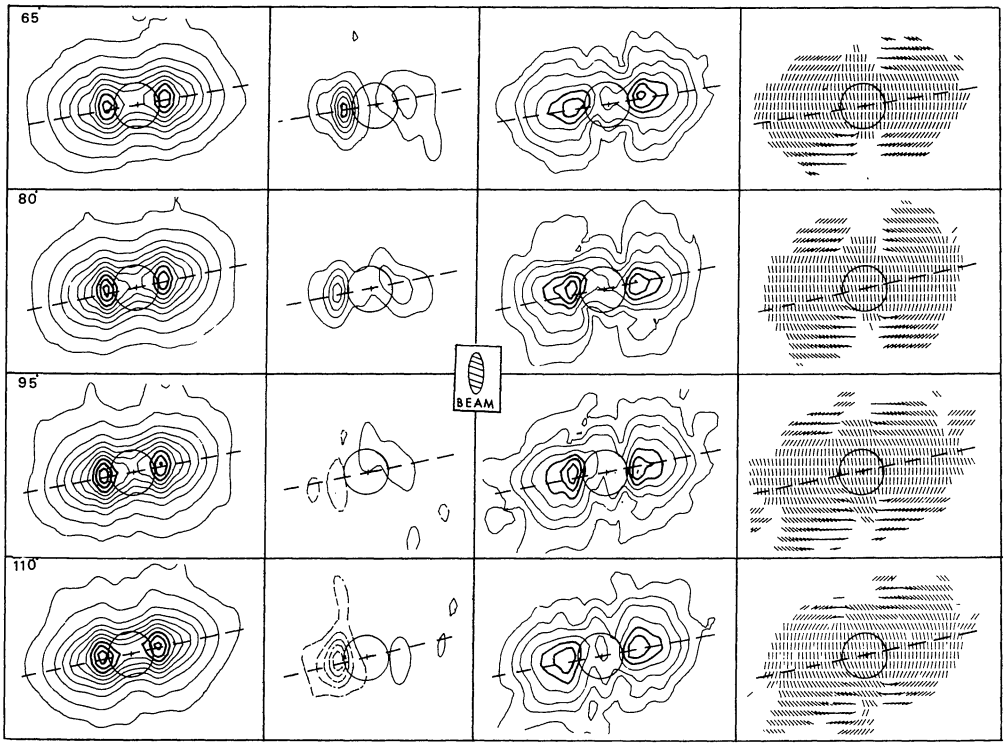

Fig. 6b

Fig. 6a–f. Two-dimensional maps of Jupiter: indicated are from left to right maps of the total intensity, circular and linear polarization fluxes and a vector diagram of the magnetic field of Jupiter. The magnetic longitude of the central meridian (Syst. III 1965.0) is indicated in the upper left corner of each series of 4. The contour values in mJy/beam are: I: 7.5 (lower contour); 50–850 in steps of 100. V: 1.50–17.25 in steps of 2.25. Dotted contours indicate left handed, fully drawn contours right handed circular polarization. $(Q^2+U^2)^{1/2}$: 7.5 (lower contour); 25, 50–250 in steps of 50. The contours belonging to the three highest values in all three kind of maps are drawn with heavy lines. The beam area is 18.093 sample points. The grid spacing is 4.″186 ($=0.177\,R_j$) in RA and 10.″636 in Dec. One may convert the values in mJy/beam to brightness temperatures by making use of the Rayleigh-Jeans approximation to the Planck function $dS/d\Omega = 2kT/\lambda^2$ with the solid angle $d\Omega$ being equal to our beam area. The contours then represent roughly the following values: I: 9.5 K (lower contour); 65–1065 K in steps of 125 K. V: 1.9–21.5 K in steps of 2.8 K. $(Q^2+U^2)^{1/2}$: 9.5 K (lower contour), 32, 65–325 K in steps of 65 K

three highest values are drawn with heavy lines. It is striking that at some longitudes where we expect to see this region on one side of the disk (i.e. $\lambda \sim 110°$–$140°$) it is hardly detected. The maps from 1973 presented in Paper I show this same feature. As indicated below this fact most likely is due to higher order terms in Jupiter's field and will be compared with model calculations in Paper III (see below).

The circularly polarized flux is a measure of the magnetic field component directed along the line of sight. Its intensity is related to the square root of the strength of the field along this line and its

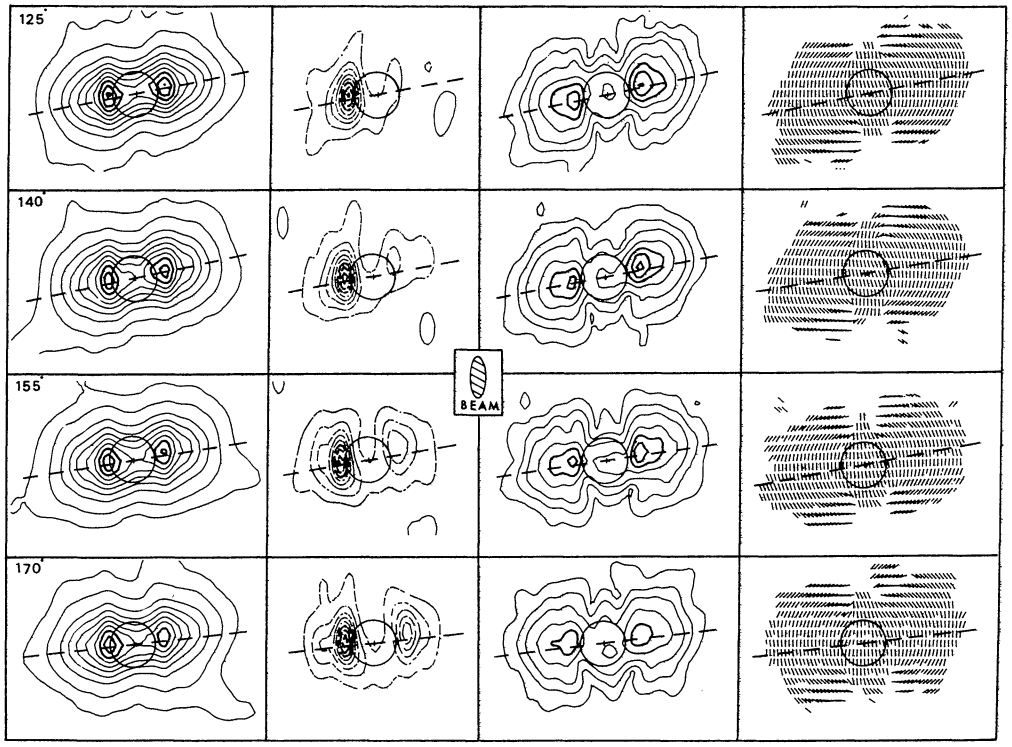

Fig. 6c

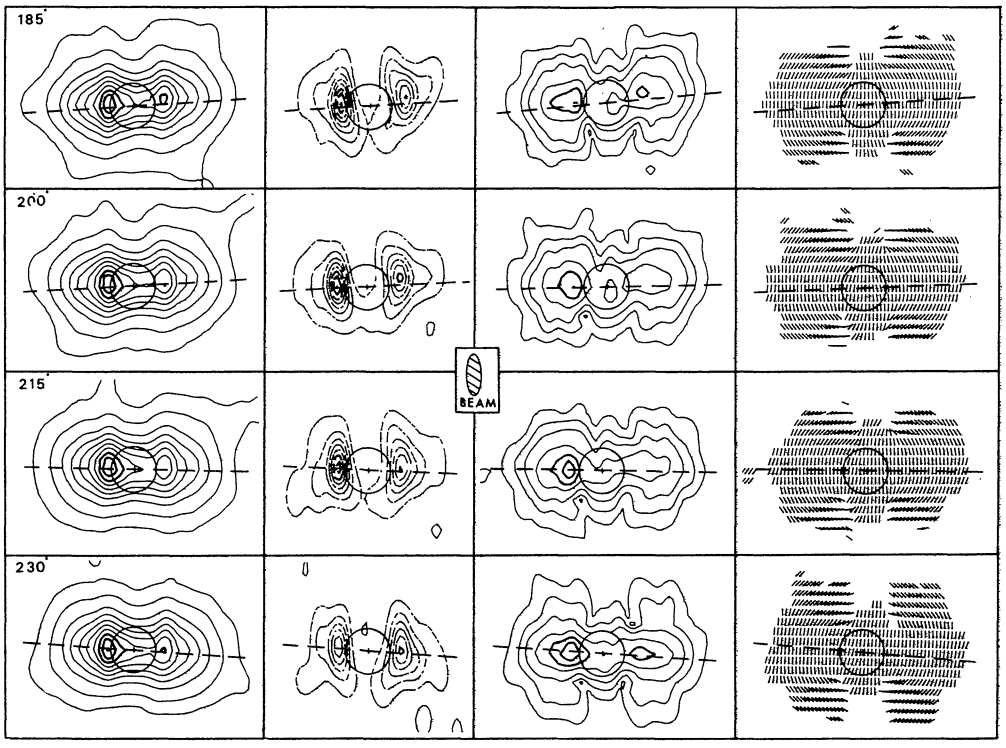

Fig. 6d

sign shows whether the field is directed towards us (right handed polarization – positive sign) or away from us (left handed polarization – negative sign). It is generally assumed, as mentioned in Sect. 3.1 that most electrons are near the magnetic equator with pitch angles near 90°. Assuming a pure dipolar field we expect the Stokes parameter V to be symmetric on both sides of the disk with maxima at the longitudes of extreme magnetic latitudes, Φ_m, and zero polarization at $\Phi_m = 0°$. Figure 6 however shows very large asymetries between both sides of the disk which strongly indicates a distortion of the magnetic equator and hence a modulation of the beaming pattern, due to higher order terms in Jupiter's field. Taking into account a region of enhanced emissivi-

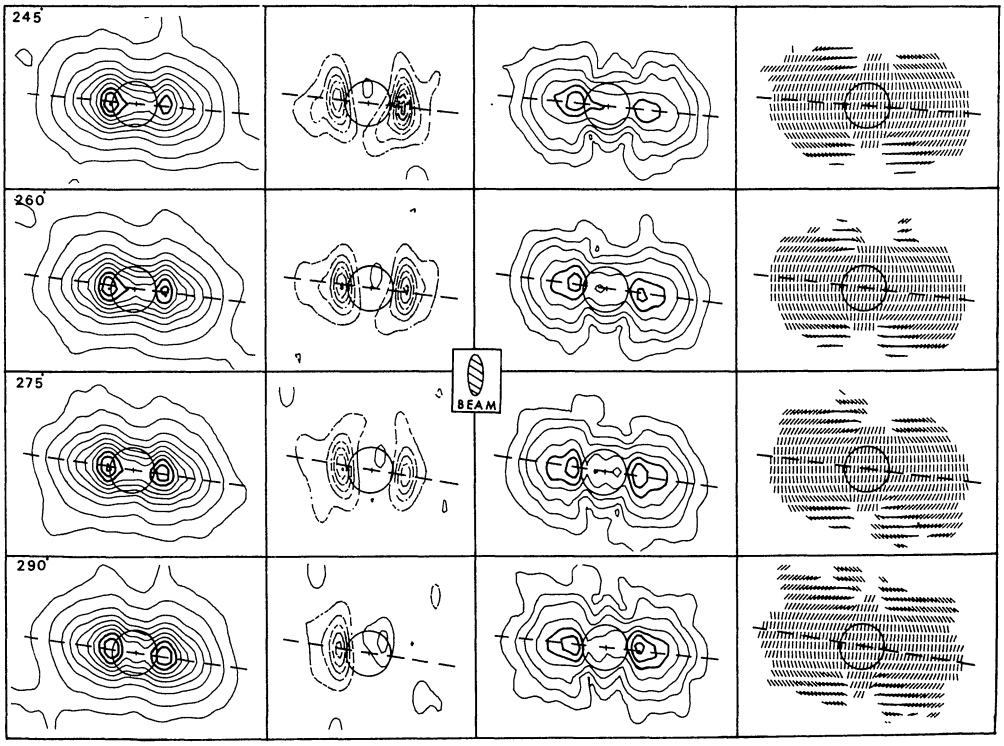

Fig. 6e

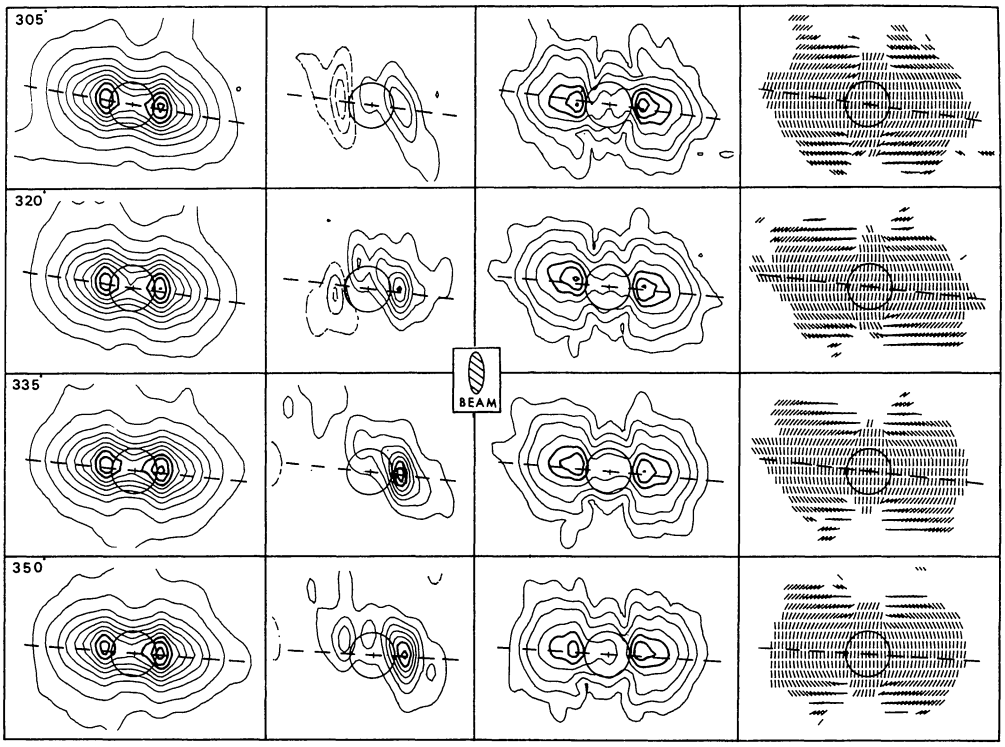

Fig. 6f

ty at $\lambda \sim 200°$–$300°$ it can be shown that existing multipole models based upon the Pioneer 10 and 11 data (Smith et al., 1976; Acuna and Ness, 1976) give a qualitative agreement between the variation with longitude of the circularly polarized flux and the difference in this flux as well as in S and P_L, between both sides of the belt. The necessity for such a multipole field model to match the radio data was already suggested by Gerard (1976).

In order to really compare these multipole magnetic field models with our data a computer program has been written which calculates the synchrotron radiation received from such a field in all four Stokes parameters, for different electron distributions in both energy and pitch angle. A detailed description of this program with calculations which best fit (particular features in) our Jovian maps will be published in Paper III (de Pater, in

preparation). Models and the integrated data for various epochs will also be compared to confirm (or reject) suggestions made in Sect. 3.1 concerning the multipole character of the field.

Having a good model for the synchrotron radiation one can subtract its contribution from the total observed intensity to define the thermal disk temperature with an accuracy much better than previously obtained (Paper I; Branson, 1968). Making a preliminary estimate for this temperature from the maps shown in Fig. 6 assuming a "mean" dipolar field model for Jupiter and using the two different methods described in Paper I, we find a temperature $T_D \sim 320 \pm 20$ K. This implies an ammonia mixing ratio of $\sim 5\,10^{-4}$ for a convective model atmosphere with solar abundances for all the other chemical elements (Gulkis, 1973).

4. Conclusions

The variation with longitude of the total intensity and linearly and circularly polarized flux of the integrated radiation is in first order consistent with a beaming pattern expected for a dipole model in which the electron pitch angle distribution is concentrated towards 90°. Small deviations may be caused by higher order terms in addition to the dipolar field of Jupiter. The existence of such terms is clearly shown in the two-dimensional maps presented in this paper at distances $\lesssim 2R_j$ from the center. These maps confirm the existence of the "hot region" at $\lambda_{III} \sim 250°$–$260°$ and its asymmetries give further information on the multipole terms of the magnetic field. A preliminary estimate for the thermal disk temperature of 320 ± 20 K is derived from the data, which is a little higher than the value found by Pater and Dames (1979). This temperature differs less from the ~ 400 K predicted by Gulkis (1973) for a convective model atmosphere with solar abundances for all chemical elements. The temperature estimated here requires an ammonia mixing ratio about 3 times higher than the solar value of $1.5\,10^{-4}$ to match a temperature profile for a convective model atmosphere.

Acknowledgements. Suggestions, advice and continued encouragement during the reduction of the data from R. S. le Poole are gratefully acknowledged. I also would like to express my thanks to K. W. Weiler for valuable discussions and advice concerning the calibration and handling of the data. Suggestions, comments and encouragement from J. R. Dickel are highly appreciated and I want to thank H. van der Laan for his initiative in acquiring NASA support for this research. I thank the Westerbork telescope and reduction groups for their careful help in the data observation and reduction and especially K. W. C. Lugtenborg who always was willing to solve problems with the "standard" reduction programs. The Westerbork Radio Observatory is operated by the Netherlands Foundation for Radio Astronomy with the financial support of the Netherlands Organization for the Advancement of Pure Research (Z.W.O.). This research was supported in part by the National Aeronautics and Space Administration, Grant NSG-7264.

References

Acuna, M.H., Ness, N.F.: 1976, in *Jupiter*, p. 830, ed. T. Gehrels, University of Arizona Press, Tucson, Arizona
Baars, J.W.M., Hooghoudt, B.G.: 1974, *Astron. Astrophys.* **31**, 323
Berge, G.L., Gulkis, S.: 1976, in *Jupiter*, p. 655, ed. T. Gehrels, University of Arizona Press, Tucson, Arizona
Berge, G.L., Seielstad, G.A.: 1972, *Astron. J.* **77**, 810
Branson, N.J.B.A.: 1968, *Monthly Notices Roy. Astron. Soc.* **139**, 155
Brouw, W.N.: 1975, *Methods in Comput. Phys.* **14**, 131
Casse, J.L., Muller, C.A.: 1974, *Astron. Astrophys.* **31**, 333
Clarke, J.N.: 1970, *Radio Sci.* **5**, 529
Degioanni, J.J.C.: 1974, *Icarus* **23**, 66
De Pater, I., Dames, H.A.C.: 1979, *Astron. Astrophys.* **72**, 148 (Paper I)
Frank, L.A., Ackerson, K.L., Wolfe, J.H., Mihalov, J.D.: 1976, *J. Geophys. Res.* **81**, 457
Gérard, E.: 1976, *Astron. Astrophys.* **50**, 353
Gulkis, S.: 1973, *Space Sci. Rev.* **14**, 497
Gulkis, S., Gary, B., Klein, M., Stelzried, C.: 1973, *Icarus* **18**, 181
Högbom, J.A.: 1974, *Astron. Astrophys. Suppl.* **15**, 417
Högbom, J.A., Brouw, W.N.: 1974, *Astron. Astrophys.* **33**, 289
Morris, D., Berge, G.L.: 1962, *Astrophys. J.* **136**, 276
Morris, D., Berge, G.L.: 1964, *Astron. J.* **69**, 641
Neidhöfer, J., Booth, R.S., Morris, D., Wilson, W., Biraud, F., Ribes, J.C.: 1977, *Astron. Astrophys.* **61**, 321
Roberts, J.A., Komesaroff, M.M.: 1965, *Icarus* **4**, 127
Roberts, J.A., Komesaroff, M.M.: 1976, *Icarus* **29**, 455
Smith, E.J., Davis, L., Jr., Jones, D.E.: 1976, in *Jupiter*, p. 788, ed. T. Gehrels, University of Arizona Press, Tucson, Arizona
Thorne, K.S.: 1963, *Astrophys. J. Suppl.* **8**, 1
Thorne, K.S.: 1965, *Radio Sci.* **69** D, 1557
van Someren Greve, H.W.: 1974, *Astron. Astrophys. Suppl.* **15**, 343
Weiler, K.W.: 1973, *Astron. Astrophys.* **26**, 403
Weiler, K.W., Raimond, E.: 1976, *Astron. Astrophys.* **52**, 397
Wilson, A.S., Weiler, K.W.: 1976, *Astron. Astrophys.* **49**, 357